

Relevance of the Basset history term for Lagrangian particle dynamics

Julio Urizarna-Carasa,¹ Daniel Ruprecht,¹ Alexandra von Kameke,² and Kathrin Padberg-Gehle³

¹*Lehrstuhl Computational Mathematics, Institut für Mathematik, Technische Universität Hamburg, Hamburg, Germany*

²*Heinrich-Blasius-Institute, Faculty of Engineering and Computer Science, Hamburg University of Applied Sciences, Hamburg, Germany*

³*Applied Mathematics, Institute for Mathematics and its Didactics, Leuphana University Lüneburg, Lüneburg, Germany*

(*Electronic mail: padberg@leuphana.de.)

(*Electronic mail: alexandra.vonkameke@haw-hamburg.de)

(*Electronic mail: ruprecht@tuhh.de)

(Dated: 2 July 2024)

The movement of small but finite spherical particles in a fluid can be described by the Maxey-Riley equation (MRE) if they are too large to be considered passive tracers. The MRE contains an integral "history term" modeling wake effects, which causes the force acting on a particle at some given time to depend on its full past trajectory. The history term causes complications in the numerical solution of the MRE and is therefore often neglected, despite both numerical and experimental evidence that its effects are generally not negligible. By numerically computing trajectories with and without the history term of a large number of particles in different flow fields, we investigate its impact on the large-scale Lagrangian dynamics of simulated particles. We show that for moderate to large Stokes numbers, ignoring the history term leads to significant differences in clustering patterns. Furthermore, we compute finite-time Lyapunov exponents and show that, even for small particles, the differences in the resulting scalar field from ignoring the BHT can be significant, in particular if the underlying flow is turbulent.

Neglecting the Basset history term in the Maxey-Riley equation can cause significant distortions not only of the trajectories of individual particles but also of the macroscopic Lagrangian dynamics.

I. INTRODUCTION

Fluid motion is all around us, in the ocean, in the atmosphere, in industrial installations and in everyday life. Oftentimes, the fluid carries other materials with it, be it plankton, buoys, dust, particulate matter or any other type of small particulate pieces of immiscible material that does not dissolve in the carrier liquid. If the volume fraction of the particulate pieces is low, it can be assumed that they move in isolation and do not collide or affect each other's movement. Furthermore, if their mass fraction is low, the effect they have on the overall flow field of the carrier phase can be neglected. Thorough discussions of the many different aspects of the mathematical description of the motion of inertial particles and real world applications can be found in the literature¹.

The equation of motion for inertial but small particles that emerges from an inspection of the acting forces is called the Maxey-Riley equation (MRE)². The MRE accounts for the Basset history force, which models the influence of the particle's past accelerations on its present motion. The equation is valid for particles of intermediate size that are too large to be considered passive tracers but not so large that they significantly disturb the fluid or that surface effects become important. The alternative is using a fully coupled fluid-structure interaction model, which, while detailed and realistic, requires massive computational effort and access to a powerful high-performance computing system³.

Mathematically, the MRE is a second order integro-differential equation. The integral or Basset history term (BHT), which captures the history force, is difficult to handle numerically due to its non-local nature and is thus typically ignored^{4,5}. However, depending on the size and density of the particle, ignoring the history term changes the simulated trajectories significantly⁶⁻⁸. The importance of the BHT for matching simulations of particle trajectories to experiments has also been confirmed: Candelier et al.⁹ investigate the impact of the BHT experimentally to elucidate how a particle is ejected out of a vortex flow and find that "calculations without history force overestimate particle ejection". Similar observations have been made in simulations¹⁰.

In many applications, one is interested in the dynamics of ensembles of particles rather than in single particle trajectories. Such a macroscopic view on Lagrangian particle dynamics is particularly relevant in the context of studying transport and mixing processes. Lagrangian coherent structures (LCS) form the time-dependent skeleton of the flow, encompassing regions of stretching and folding that enhance or mitigate particle transport¹¹. Many different computational approaches have been developed over the past almost three decades to identify coherent flow structures, such as LCS or coherent sets, and to study their dynamics, including bifurcations^{12–14}. Finite-time Lyapunov exponents (FTLE) are often heuristically used to highlight regions of different dynamical behavior. Inertial particles are known to interact with the underlying flow skeleton and tend to concentrate along different coherent structures, for example vortices, depending on their material properties such as size and density^{15,16}. There are several studies that compare the FTLE fields for ideal tracers that exactly follow the underlying flow with those computed for inertial particles. They found that the corresponding flow structures can be crucially different^{17,18}. However, these studies did not consider the history term and the specific influence of the BHT on the LCS has not yet been studied. Therefore, this paper investigates the differences in flow structures for particle dynamics simulated with and without Basset term. For this, we make use of recent mathematical developments in the numerical solution of the Maxey-Riley equation with history term^{6,19}, which has opened the door to the simulation of many particles²⁰.

A. Contributions

Our paper investigates the impact of neglecting the BHT on the macroscopic dynamics of simulated Lagrangian particles. We retain the assumption that the flow influences the particle motion but that there is no impact on the background flow, allowing us to use the MRE as model. We study the resulting flow patterns in a controlled setting for three example systems, the double gyre²¹, the Bickley jet²², and a Faraday flow, a two-dimensional, fully turbulent, experimentally measured flow^{23,24}.

We compare particle dispersion and finite time Lyapunov exponents (FTLE) for particle trajectories computed with and without history term with different Stokes numbers and densities. Our analysis demonstrates that, even for moderate Stokes numbers of unity or more, the particle dispersion patterns revealed by the FTLE are noticeably changed by ignoring the history term. In particular, our results suggest that simulations without BHT produce results that are comparable

to flows with an effective Stokes number that is larger than used value. This is very much in accordance with previous findings^{9,10}. Our results also suggest that care must be taken when attempting to predict flow regimes, or sudden changes thereof, that involve inertial particle dynamics. Important examples would be the oil spill in the Gulf of Mexico, ocean search-and-rescue²⁵, or the splitting of the polar vortex.

B. Outline

Section II introduces the the Maxey-Riley equation, its numerical solution and the computation of finite-time Lyapunov exponents. Section III describes the three flow fields used in our study. In Section IV we present the results of our investigation. First we analyse and compare the final particle positions and their preferential concentration. Second, we present FTLE fields for a range of different parameter configurations. Conclusions and a summary can be found in Section V.

II. BACKGROUND

In this section, we introduce the Maxey-Riley equation (MRE) and its numerical treatment as well as the equation and approximations used to obtain the finite-time Lyapunov exponents (FTLE).

A. The Maxey-Riley Equation (MRE)

Throughout this work, we consider (i) spherical particles with a small radius compared to the flow dimensions, which guarantees a small particle Reynolds number⁴, (ii) one-way interactions between particles and fluid, so that the flow influences the particle dynamics but not the other way round⁶ and, (iii) no particle collisions. Under these assumptions, particle trajectories can be modeled using the MRE in nondimensionalized form

$$\dot{\mathbf{v}} = \frac{1}{R} \frac{D\mathbf{u}}{Dt} + \tag{1a}$$

$$- \frac{1}{RS} (\mathbf{v} - \mathbf{u}) + \tag{1b}$$

$$- \frac{1}{R} \sqrt{\frac{3}{\pi S}} \left\{ \frac{1}{\sqrt{t}} (\mathbf{v}(t_0) - \mathbf{u}(t_0)) + \int_{t_0}^t \frac{\mathbf{v}(s) - \mathbf{u}(s)}{\sqrt{t-s}} ds \right\}, \tag{1c}$$

as adapted by Prasath et al.⁶ from the original paper by Maxey and Riley², where $\mathbf{v} := \dot{\mathbf{x}}(t)$ is the particle's absolute velocity, $\mathbf{x}(t)$ the particle's position and $\mathbf{u} := \mathbf{u}(\mathbf{x}(t), t)$ the value of the Eulerian velocity field at the particle's position. Note that we only consider particles moving in a plane so that $\mathbf{x}(t), \mathbf{v}(t) \in \mathbb{R}^2$ throughout. Further,

$$\beta := \frac{\rho_p}{\rho_f}, \quad R := \frac{1 + 2\beta}{3}, \quad S := \frac{1}{3} \frac{a^2}{\nu T}, \quad (2)$$

where ρ_p, ρ_f correspond to the particle and fluid densities, a is the particle's radius, ν its kinematic viscosity and T the time scale of the flow. The effective density ratio R controls buoyancy and inertia and accounts for the added mass effect that arises because the particle accelerates surrounding fluid and carries it along its path. Heavier particles that are denser than the carrier fluid with $\beta > 1$, where also $R > 1$, are less susceptible to the fluid forces than lighter particles, i.e. $\beta < 1$ with $R < 1$, compare for the particle acceleration and first term in (1a).

The nondimensional parameter S in (1) characterizes the particle radius with respect to the flow dimensions. We refer to S as the Stokes number since it compares the particle relaxation timescale $\tau_p = \frac{a^2}{\nu}$ to a flow timescale T . Often, T is chosen to be the time scale of the mean flow or eddy turnover time but setting it properly requires some care²⁶. We compute LCS for values of $S = 0.1$, $S = 1$ and $S = 10$. This is in line with values studied in other papers^{7,27}.

However, note that the Stokes numbers in both references correspond to the experimental Stokes number

$$S_{exp} = S \cdot \frac{2 \rho_p}{3 \rho_f} = \frac{2 a^2 \rho_p}{9 \nu \rho_f} \frac{1}{T} = \frac{2 a^2 \rho_p U L}{9 L^2 \rho_f \nu} = \frac{2 a^2 \rho_p}{9 L^2 \rho_f} Re_f \quad (3)$$

with U, L and Re_f being the flow velocity and timescales and the corresponding flow Reynolds number. The experimental Stokes number is slightly different from the non-dimensional S we prescribe here. Experimentalists tend to use S_{exp} , which also incorporates the density ratio, to examine how closely the particle follows the flow²⁸. This Stokes number arises as a prefactor of the Stokes drag term, not mingled with the added mass term, in the non-dimensionalized Maxey-Riley equation and is widely used in the literature²⁹. It allows to account for non-Stokesian drag when $Re > 1$ by using the expression $S_{exp} = f \cdot \frac{a^2 \rho_p}{\nu \rho_f} \frac{1}{T}$, where f is a factor that depends on the particle Reynolds number $f = f(Re_p)$ ³⁰. For our density ratios of $\beta = \rho_p/\rho_f = 2/3$ and $\beta = 4/3$, a value of $S_{exp} = 10$ as studied by Olivieri et al.⁷ corresponds to a Stokes number as used in this article of $S = 22.50$ and $S = 11.25$ respectively.

The MRE is derived from Newton's second law for the particle movement and a velocity field approximation of the influence of the particle on the local flow from potential flow theory under

creeping flow assumption. This implies that the validity of the formula is only guaranteed for low particle Reynolds numbers with low relative velocities. Terms on the right hand side of equation (1) correspond to different forces acting on the particle. Term (1a) are the forces acting on a particle in an unperturbed fluid lumped up with the added mass effect. Term (1b) is the Stokes drag. Term (1c), the so-called Basset History Term (BHT), accounts for the effects of the lagging boundary layer around the sphere³¹.

Since the aim of our work is to examine the influence of the history force, we neglect the so-called Faxen corrections that model the influence of the particle's finite size and scale with the curvature of the velocity field. However, for larger particles, the Faxen corrections should be considered as they have been shown to play a crucial role in shear flows³² where they cause fluctuations in the particle's velocity and thus a relative velocity between particle and fluid flow. In (1), since we assume that the particle initially has same velocity as the fluid, only particles with buoyancy $R \neq 1$ will produce non-zero relative velocities and cause the trajectories of particles with and without history force to deviate.

B. Numerical solution of the MRE

The BHT is made up of a history integral with a singular kernel. This term changes the MRE from an ordinary differential into an integro-differential equation that is not easily solvable either analytically or numerically. For this reason, the term is often omitted³³, modified^{34–37} or approximated^{38–41}. Several numerical approximations, based on quadrature schemes, were obtained by Van Hinsberg et al.⁴¹ and Daitche⁴². However these schemes become storage-intensive for large time grids. In 2019, Prasath et al. showed that the MRE can be written "as a forced, time-dependent Robin boundary condition of the one-dimensional diffusion equation"⁶ and provided a storage-efficient numerical scheme. In this paper, trajectories with BHT are calculated with the second order finite-difference, IMEX solver (FD2 + IMEX2) by Urizarna-Carasa et al.¹⁹ that relies on Prasath's reformulation. The scheme uses the second order spatial discretization provided by Koleva⁴³ coupled with a second order Midpoint IMEX method given by Ascher et al.⁴⁴ to solve the reformulated MRE. Trajectories without BHT are calculated with the explicit adaptive Runge-Kutta method of order 5(4) provided by the *solve_ivp* solver of Python's SciPy⁴⁵ library, using a relative and absolute tolerance of 10^{-8} . For verification, trajectories without BHT were compared against the Leap-Frog method, whereas trajectories with BHT were compared against Daitche's

3rd order method⁴². All figures shown in this paper can be reproduced using the provided code⁴⁶.

C. Finite-time Lyapunov exponents (FTLE)

Finite-time Lyapunov exponents (FTLE) are a measure of the exponential growth of an infinitesimal perturbation in the initial condition under the action of the dynamical system. FTLE fields have become a popular, heuristic tool in nonlinear dynamics to highlight organizing structures in phase space such as invariant manifolds of hyperbolic objects or Lagrangian coherent structures in time-dependent flows^{11,21}. Typically FTLE have large values for repelling LCS when computed in forward time, and for attracting ones when computed in backward time. Close to zero values are frequently observed for elliptic motion, such as in the center of vortices. While more sophisticated approaches have been developed to identify LCS¹¹, we use FTLE as a convenient and meaningful scalar field that allows to visualize regions of different dynamical behavior.

The expression to compute the FTLE of a flow field at a position \boldsymbol{x} is

$$\sigma_{t_0}^t(\boldsymbol{x}) := \frac{1}{|t - t_0|} \ln \left(\sqrt{\lambda_{\max}(\Delta)} \right), \quad (4)$$

where $\boldsymbol{x} = (x, y)^T$ is the position vector, $\lambda_{\max}(\Delta)$ is the largest eigenvalue of the Cauchy-Green deformation tensor $\Delta := (D\Phi_{t_0}^t)^* D\Phi_{t_0}^t$, and $D\Phi_{t_0}^t$ is the deformation gradient of the flow map. The flow map $\Phi_{t_0}^t$ is evaluated by integrating (1) using either *solve_ivp* or the FD2 + IMEX2 scheme described above. $D\Phi_{t_0}^t$ can either be obtained by solving a variational equation or by approximating the derivative numerically using finite-differences. The latter is straightforward to implement and thus used in most cases, even when a kinematic model is available.

FTLE methods have also been applied in the context of inertial particle dynamics as described by the Maxey-Riley equation^{16–18} and perturbations both in positions and velocities have been taken into account to define inertial finite-time Lyapunov exponents (iFTLE). In that case not only partial derivatives with respect to positions and velocities would make up the deformation gradient of the flow map, resulting in a 4×4 matrix in the case of a two-dimensional flow velocity field. Since our aim is to study the influence of the Basset history term on particle dynamics and transport properties by comparing flow structures computed with and without history term we neglect perturbations in the initial velocities and the flow map only considers the particle positions. Therefore, in our study, $D\Phi_{t_0}^t$ is a 2×2 deformation gradient.

Numerical particle trajectories can only be calculated at discrete points in space. Thus, the

entries of the deformation gradient of a particle in an interior point of the domain (position $\mathbf{x}_{i,j}$ in the stencil shown in Figure 1) are approximated by the second order finite-difference scheme¹⁷

$$D\Phi_{t_0}^t|_{1,1} \approx \frac{x_{i+1,j}(t_{end}) - x_{i-1,j}(t_{end})}{x_{i+1,j}(t_0) - x_{i-1,j}(t_0)}, \quad (5a)$$

$$D\Phi_{t_0}^t|_{1,2} \approx \frac{x_{i,j+1}(t_{end}) - x_{i,j-1}(t_{end})}{y_{i,j+1}(t_0) - y_{i,j-1}(t_0)}, \quad (5b)$$

$$D\Phi_{t_0}^t|_{2,1} \approx \frac{y_{i+1,j}(t_{end}) - y_{i-1,j}(t_{end})}{x_{i+1,j}(t_0) - x_{i-1,j}(t_0)}, \quad (5c)$$

$$D\Phi_{t_0}^t|_{2,2} \approx \frac{y_{i,j+1}(t_{end}) - y_{i,j-1}(t_{end})}{y_{i,j+1}(t_0) - y_{i,j-1}(t_0)}. \quad (5d)$$

At the boundaries, where values outside the initial domain are not available, a first order approximation is used. Following Shadden et al.²¹, all FTLE plots in this paper show $\sigma_{t_0}^t(\mathbf{x})|t - t_0|$.

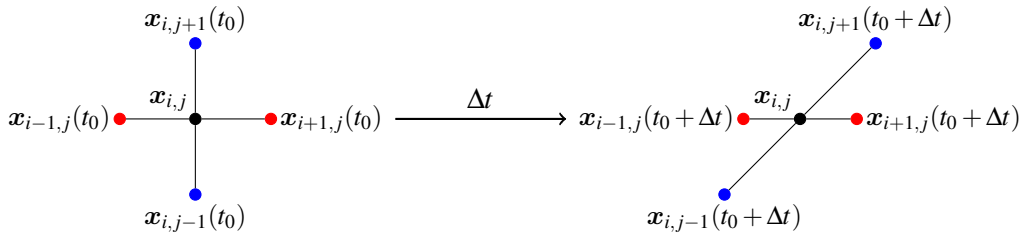


FIG. 1. Stencil used for the calculation of the FTLE $\sigma_{t_0}^t(\mathbf{x}_{i,j})$ at position $\mathbf{x}_{i,j}$ and an example of the translation of the particles in the stencil after a time Δt .

III. FLOW FIELDS

This section introduces the three flow fields that will serve as test cases for our study. Our choice of two-dimensional velocity fields includes the frequently studied kinematic double gyre and Bickley jet as well as a Faraday flow obtained from experimental measurements.

In all three fields, particle trajectories are integrated from $t_0 = 0$ until $t_{end} = 10$ with a timestep of $\Delta t = 0.01$. Particles always start with zero relative velocity, that is $\mathbf{v}(t_0) = \mathbf{u}(\mathbf{x}(t_0), t_0)$.

1. Double gyre

The double gyre is a popular example in the study of the FTLEs. It is a simplified model of a pattern that occurs in geophysical flows²¹. The velocity flow field is obtained from the stream-

function

$$\psi(x, y, t) = A \sin(\pi f(x, t)) \sin(\pi y), \quad (6)$$

where

$$f(x, t) = a(t)x^2 + b(t)x, \quad (7a)$$

$$a(t) = \varepsilon \sin(\omega t), \quad (7b)$$

$$b(t) = 1 - 2\varepsilon \sin(\omega t), \quad (7c)$$

with $A = 0.1$, $\varepsilon = 0.25$, $\omega = \frac{\pi}{5}$.

We consider 20301 particles starting in the spatial domain $M = [0, 2] \times [0, 1]$. Particles are distributed in 201 vertical lines by 101 horizontal lines, so that adjacent particles are separated by a distance of 0.01. Ideal passive tracers cannot leave the domain M but inertial particles can cross the domain walls. Particles leaving the domain boundaries will continue being affected by the flow field, since the double gyre is defined for all point in \mathbb{R}^2 .

2. Bickley Jet

As our second example, we consider the Bickley jet proposed by Rypina et al.²². It is defined by the streamfunction

$$\Psi(x, y, t) = -U_0 L \tanh\left(\frac{y}{L}\right) + \quad (8a)$$

$$+ \sum_{i=1}^3 A_i U_0 L \operatorname{sech}^2\left(\frac{y}{L}\right) \cos(k_i x - \sigma_i t), \quad (8b)$$

and serves as an idealized model of stratospheric flow. We use same the parameter values as Hadjighasem et al.^{47,48}, i.e. $U_0 = 5.414$, $A_1 = 0.0075$, $A_2 = 0.15$, $A_3 = 0.3$, $L = 1.770$, $c_1/U_0 = 0.1446$, $c_2/U_0 = 0.205$, $c_3/U_0 = 0.461$, $k_1 = 2/r_e$, $k_2 = 4/r_e$, $k_3 = 6/r_e$ where $r_e = 6.371$ as well as $\sigma_i = c_i k_i$, $i = 1, 2, 3$. For our choice of parameters and when considered on a cylinder, the system exhibits a meandering central jet and three regular vortices on each side of the jet.

In our study, 16281 initial conditions are chosen in the rectangle $M = [0, 20] \times [-4, 4]$. Particles are distributed within 81 horizontal lines by 201 vertical lines, so that again there is a separation of 0.01 among adjacent particles. No periodic boundary conditions are imposed, so particles are allowed to leave the initial domain and disperse over \mathbb{R}^2 . In contrast to other representations of the Bickley jet, this field does not thus represent a cylinder.

3. *Faraday flow*

The Faraday flow field is an experimentally-measured flow field. It is obtained from the surface of a 2 mm-thick layer of distilled water in a cylindrical container of 290 mm diameter as it is vertically shaken with a monochromatic sinusoidal signal at a frequency of 50 Hz at a measured forcing acceleration of $a = 1.6g$ which corresponds to a supercriticality of $\varepsilon = 0.04$ ²³. This movement produces the so-called Faraday waves, quasi-standing waves over the fluid's surface, and a turbulent space- and time-dependent 2D-velocity field which exhibits all characteristics of two-dimensional turbulence⁴⁹. Energy is injected into the flow at a scale of half the Faraday wavelength which corresponds to the spatial scale of the smallest occurring vortices. In contrast to three-dimensional turbulence, energy is passed from this scale upwards to larger scales and an inverse energy cascade is forming, distributing the energy from the forcing scale up to the system size. Therefore, above half the Faraday wavelength all vortex sizes occur, leading to effective turbulent diffusion of tracers in the flow above the forcing scale⁵⁰. The velocity field is measured using particle image velocimetry (PIV) with floating white, hollow, glass microspheres (diameter of $70\mu m$, density of $0.15g/cm^3$, Fibre Glast) to visualize the horizontal motion. The tracer particles are chosen such that they follow the fluid motion as closely as possible. A non-ionic surfactant (1% Polysorbate 80) is used in 10% or less solids solution to ensure that the particles do not aggregate and sink. The particles are recorded with a high-speed camera (pco.dimax HS2 and Carl Zeiss Makro-Planar $T * 2.8/100mm$ lens) and triggered at a frequency of 400 Hz. The details of the experimental setup are similar to those given by Colombi et al.^{23,24}. From the particle images, velocity data is obtained using PIVview (PIVTEC GmbH, Germany) and MATLAB. One set of data for the Faraday flow consists of discrete velocity values for both horizontal and velocity components, v_x and v_y , at 115×86 spatial grid points over an area of roughly $73.90 \times 55.42mm^2$ as results from a length conversion via calibration. These measurements were taken for 1056 successive time steps, resulting in a total measurement time of 42.24 s. When needed, intermediate velocity values are interpolated in space with SciPy's bivariate rectangular Spline⁴⁵. Interpolation in time is carried out using linear interpolation.

Simulated particle trajectories are computed for 40401 particles initialized in the rectangle $M \approx [0, 0.07] \times [0, 0.05]$. Particles are distributed along 201 vertical and 201 horizontal lines and are allowed to leave the initial domain, since no boundary condition is imposed. The flow field's velocity and its derivatives are set to 0 beyond the boundaries, so that particles behave as relaxing

particles after they leave the initial domain and are unable to return.

IV. NUMERICAL RESULTS

In this section, we analyze the impact of the history term first on the final distribution of particles and then on the FTLE. The flow fields we consider are a double gyre, the Bickley jet and an experimentally measured Faraday flow as described in Section III.

A. Particle clustering

For the double gyre and Bickley jet we show the final positions of all particles, first for lighter-than-fluid and then for heavier-than-fluid particles. We omit clustering plots for the Faraday flow as they do not provide significant additional insight, but they can easily be generated using the accompanying code. Finally, for all three flow fields, we state the relative average difference in the final position of particles computed with and without BHT

$$d := \frac{1}{N} \sum_{i=1}^N \left(\frac{\|x_i(t_{\text{end}}) - x_i^{\text{nobht}}(t_{\text{end}})\|_2}{\frac{1}{N} \sum_{j=1}^N \|x_j(t_{\text{end}}) - x_j(t_0)\|_2} \right). \quad (9)$$

in Table I. Here, N is the number of particles, $x_i(t_{\text{end}})$ the final position of a particle computed with the full MRE and $x_i^{\text{nobht}}(t_{\text{end}})$ the final position of the same particle computed without BHT.

The average relative difference in final positions computed with and without BHT for the double gyre and Bickley jet with $S = 0.1$ are less than 10% with standard deviations of similar order. However, for the more turbulent Faraday flow that contains flow structures spanning a large range scales, even for $S = 0.1$ we see a significant effect from the BHT. This can likely be explained by the turbulent characteristics of the Faraday flow which, due to its turbulence in space and the large fluctuations in time, has more separatrices where nearby particles get caught up in very different fates. Further, the lowest spatial scale in the Faraday flow, half the Faraday wavelength $\lambda_f/2 \approx 5\text{mm}$ is smaller when compared to the simulated particle sizes. For instance calculating the size of the simulated particle for $S = 0.1$ via

$$d_p = \sqrt{S\beta \frac{9(\lambda_f/2)^2}{2 Re_f}} \quad (10)$$

results in $d_p \approx 500\mu\text{m}$ to $800\mu\text{m}$ for β set to $2/3$ or $4/3$ respectively, which is only a factor of ten away from the injection scale $\lambda_f/2$. The approximated Reynolds number of the Faraday flow is $Re_f \approx 100$.

Average relative distance and standard deviation			
Flow field	S	$R = 7/9$	$R = 11/9$
Double gyre	0.1	0.03 ± 0.06	0.03 ± 0.05
	1	0.34 ± 0.38	0.53 ± 0.63
	10	0.65 ± 0.75	0.44 ± 0.56
Bickley jet	0.1	0.06 ± 0.11	0.07 ± 0.13
	1	0.18 ± 0.36	0.14 ± 0.23
	10	0.35 ± 0.37	0.29 ± 0.33
Faraday flow	0.1	0.29 ± 0.45	0.40 ± 0.52
	1	1.06 ± 0.76	1.20 ± 0.73
	10	2.88 ± 1.59	2.65 ± 1.45

TABLE I. Average relative distance (9) and standard deviation between the final position when computing the trajectories of particles with and without Basset history term.

For all three flow fields, for Stokes numbers of $S = 1$ and $S = 10$, the computed final position are substantially different when ignoring the BHT. Furthermore, the standard deviations suggest that there are large differences between particles in how ignoring the BHT affects their trajectories. It is clear that the BHT does not have the same effect on all trajectories but that there is a more complex process at play.

1. *Double gyre*

Figure 2 shows the positions of particles in the double gyre at the end of the simulation for Stokes numbers $S = 0.1$ (left), $S = 1$ (middle) and $S = 10$ (right) for particles that are lighter than the fluid with $R = 7/9$. Figure 3 shows the same for denser-than-fluid particles with $R = 11/9$. Upper figures show final positions when computing particle trajectories without history term while lower figures use the full MRE. Table I shows the average relative distance (9) between the final position of particles computed with and without BHT.

For the lighter-than-fluid particle with $R = 7/9$ and a small Stokes number of $S = 0.1$, there is little visible impact from the history term. However, for $S = 1$, neglecting the BHT leads to

Relevance of the Basset history term for Lagrangian particle dynamics

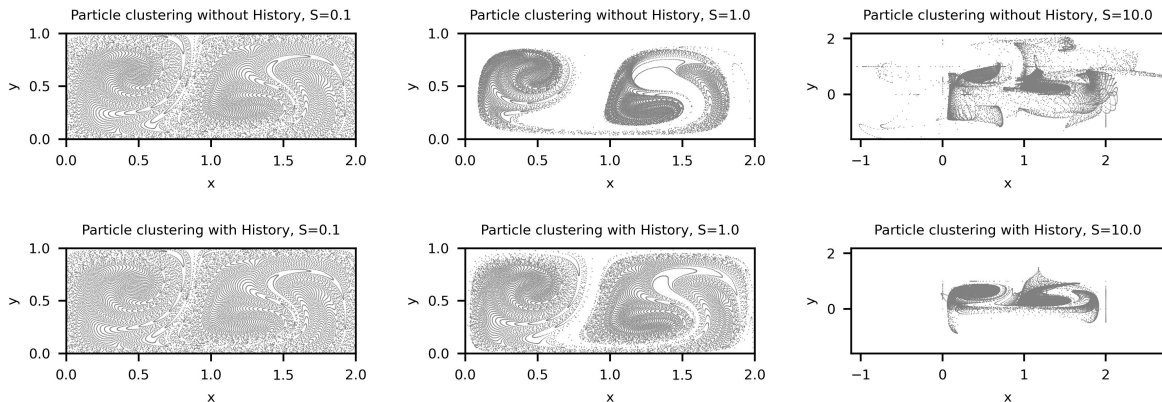


FIG. 2. Particle positions at final time $t_{end} = 10$ for the double gyre calculated without (top) and with (bottom) BHT. All particles have the same effective density ratio $R = 7/9$. Stokes numbers increase from left to right: $S = 0.1$ (left), $S = 1$ (center) and $S = 10$ (right).

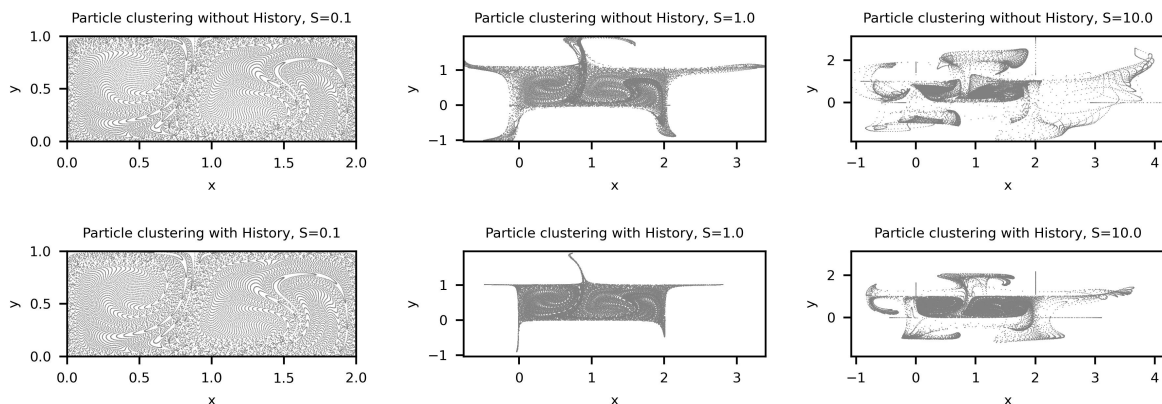


FIG. 3. Particle positions at final time $t_{end} = 10$ for the double gyre calculated without (top) and with (bottom) BHT. All particles have the same effective density ratio $R = 11/9$. Stokes numbers increase from left to right: $S = 0.1$ (left), $S = 1$ (center) and $S = 10$ (right).

much more pronounced clustering, although the patterns that form are still broadly similar. For $S = 10$, finally, clustering patterns also show significant qualitative differences. The main reason is that ignoring the BHT causes a large number of particles to escape the double gyre (note the different scaling of the y-axis in the right compared to the middle and left figure). This agrees with the findings of Candelier et al.⁹, who found that ignoring the BHT when simulating particles in a vortex flow leads to an overestimation of ejection. This could be problematic in many cases, one example being sorting particles by Stokes number using their different separation characteristics⁵¹.

The picture looks similar for the denser-than-fluid particle with $R = 11/9$. For $S = 0.1$, there is little difference between clustering patterns computed with and without BHT. Again, a visible difference emerges for $S = 1$ although for the denser-than-fluid particles the BHT leads to slightly more focused concentration patterns. The “tentacles” formed by escaping particles are much narrower when including the BHT, suggesting again that without BHT more particles are ejected from the domain. For $S = 10$ we also observe the expected accentuated ejection for the denser-than-fluid particles. The patterns formed by the particles are neater and tidier when the BHT is included, in contrast to the more erratic and dispersed patterns obtained when it is ignored. This is also in accordance with observations that neglecting the history terms leads to more complex dynamics¹⁰.

2. Bickley jet

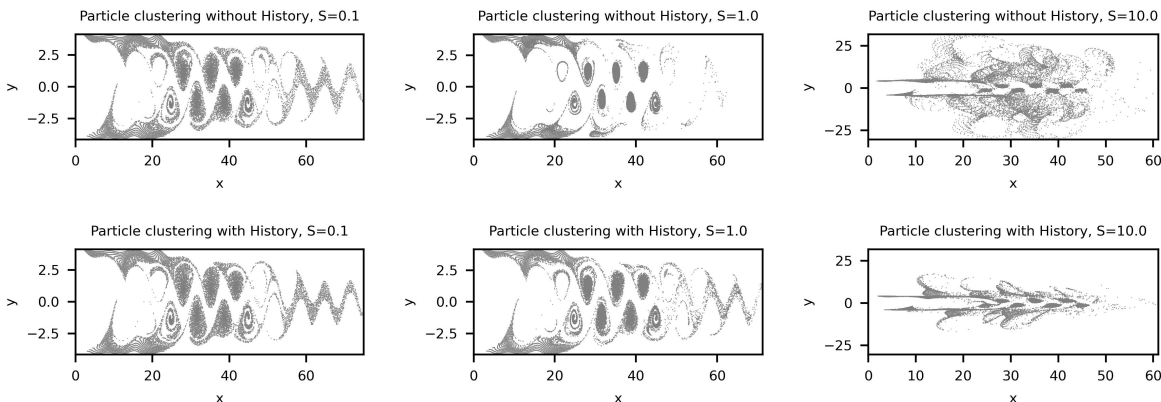


FIG. 4. Particle positions at final time $t_{end} = 10$ for the Bickley jet calculated without (top) and with (bottom) BHT. All particles have the same effective density ratio $R = 7/9$. Stokes numbers increase from left to right: $S = 0.1$ (left), $S = 1$ (center) and $S = 10$ (right).

Figure 4 shows the positions of particles in the Bickley jet at the end of the simulation for Stokes numbers $S = 0.1$ (left), $S = 1$ (middle) and $S = 10$ (right) for particles with $R = 7/9$ that are lighter than the fluid. Figure 5 shows the same for denser-than-fluid particles with $R = 11/9$.

As for the double gyre, the BHT has little impact for $S = 0.1$, both for the lighter- and denser-than-fluid particle. For lighter-than-fluid particles and $S = 1$, neglecting the BHT leads again to stronger clustering in the centers of the vortices. For the denser-than-fluid particles, this effect is reversed and ignoring the BHT leads to stronger ejection. As in the case of the double gyre, we

Relevance of the Basset history term for Lagrangian particle dynamics

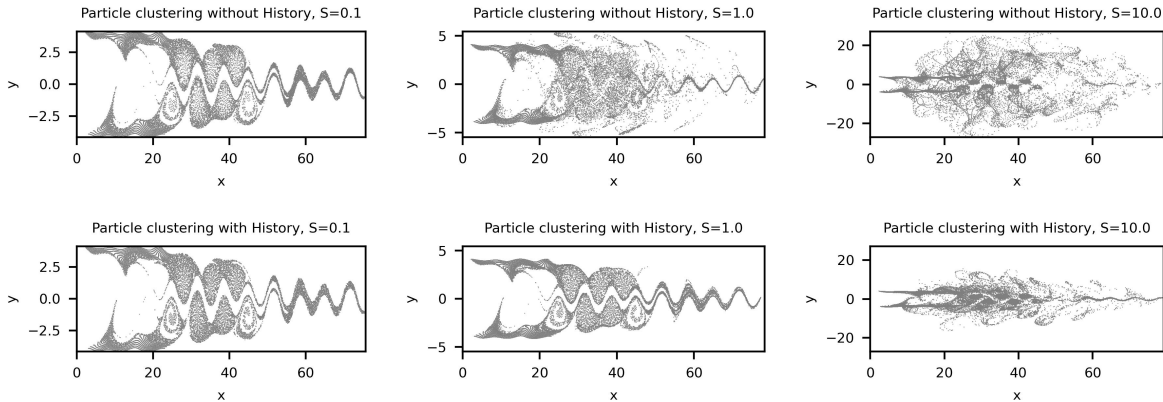


FIG. 5. Particle positions at final time $t_{end} = 10$ for the Bickley jet calculated without (top) and with (bottom) BHT. All particles have the same effective density ratio $R = 11/9$. Stokes numbers increase from left to right: $S = 0.1$ (left), $S = 1$ (center) and $S = 10$ (right).

see a lot more particles escape from the central jet into the lower and upper regions when ignoring the BHT (note the changed scaling of the y-axis in the plots for $S = 10$). Again, ignoring the BHT produces more irregular patterns, especially for larger S .

B. Finite-time Lyapunov exponents

This section shows colormap plots of the FTLE for all three flow fields. For every flow field, we show two sets of nine plots, each set showing the FTLE results obtained without and with history term as well as the difference between the two respective fields in percent for Stokes numbers $S = 0.1$, $S = 1$, $S = 10$ and density ratios $R = 7/9$ and $R = 11/9$. The relative difference between FTLEs $\Delta\sigma_{t_0,relative}^t$ is calculated from

$$\Delta\sigma_{t_0,relative}^t := 100 \frac{\sigma_{t_0,History}^t - \sigma_{t_0,Stokes}^t}{\|\sigma_{t_0,History}^t\|_{l_\infty(D)}} \quad (11)$$

where $D \subset \Omega \times [0, T]$ and $\Omega \subseteq \mathbb{R}^2$ is the spatial domain. The differences are signed and negative values correspond to areas where neglecting the BHT will increase FTLE while positive areas mean that neglecting the BHT will lead to smaller FTLE.

For $R = 1$ the FTLE fields are independent of S and, since we do not consider any effects that induce non-zero relative velocities, they agree independent of whether the BHT is present or not. We confirmed that our numerical solutions reproduce this behavior correctly but do not show any figures.

1. Double gyre

Figure 6 shows the FTLE without BHT (left), with BHT (center) and the difference between the two (right) for lighter-than-fluid particles with $R = 7/9$. From top to bottom the Stokes number changes from $S = 0.1$ to $S = 1$ and $S = 10$.

In line with the clustering plots, the impact of the BHT for $S = 0.1$ is small. The FTLE show no visible differences and agree to within a few percent. For $S = 1$, the FTLE still look qualitatively similar although some differences emerge. In particular, the region of strong divergence between the gyres shifts its position. When the Stokes number becomes even larger, at $S = 10$, we start to see substantial qualitative differences as well. Without BHT, a number of filaments of strong divergence appear that are not present in the FTLE with history term. There are now substantial differences between the two FTLE fields of up to $\pm 100\%$ in some regions.

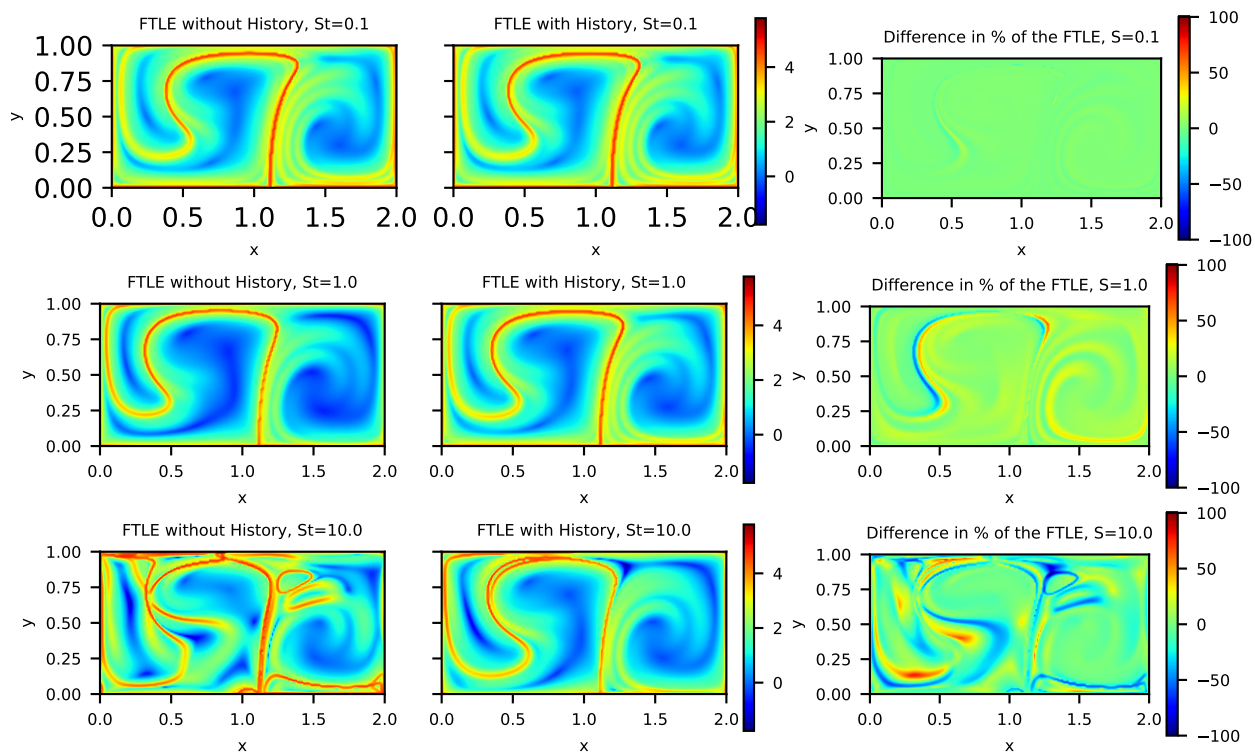


FIG. 6. FTLEs for light particles ($R = 7/9$) and three Stokes numbers, $S = 0.1$ (top), $S = 1$ (center), $S = 10$ (bottom), moving in the Double Gyre with periodic Boundary conditions. Left and center columns show the FTLEs computed with trajectories calculated without (left) and with (right) BHT. Right column shows the relative difference in the FTLE.

Figure 7 shows the same plots but for heavier-than-fluid particles with $R = 11/9$. As for the

light particle, there is little difference between the FTLE for $S = 0.1$. For $S = 1$, however, the differences between BHT and no BHT are more pronounced. While still qualitatively similar, the regions of strong separation between and around the gyres look noticeably different. Without BHT, there are three well separated filaments of strong divergence between the gyres which are much closer together and almost fused when the BHT is used. More generally, the red, high-FTLE filaments around the gyres shift away from the center of the domain when including the history term.

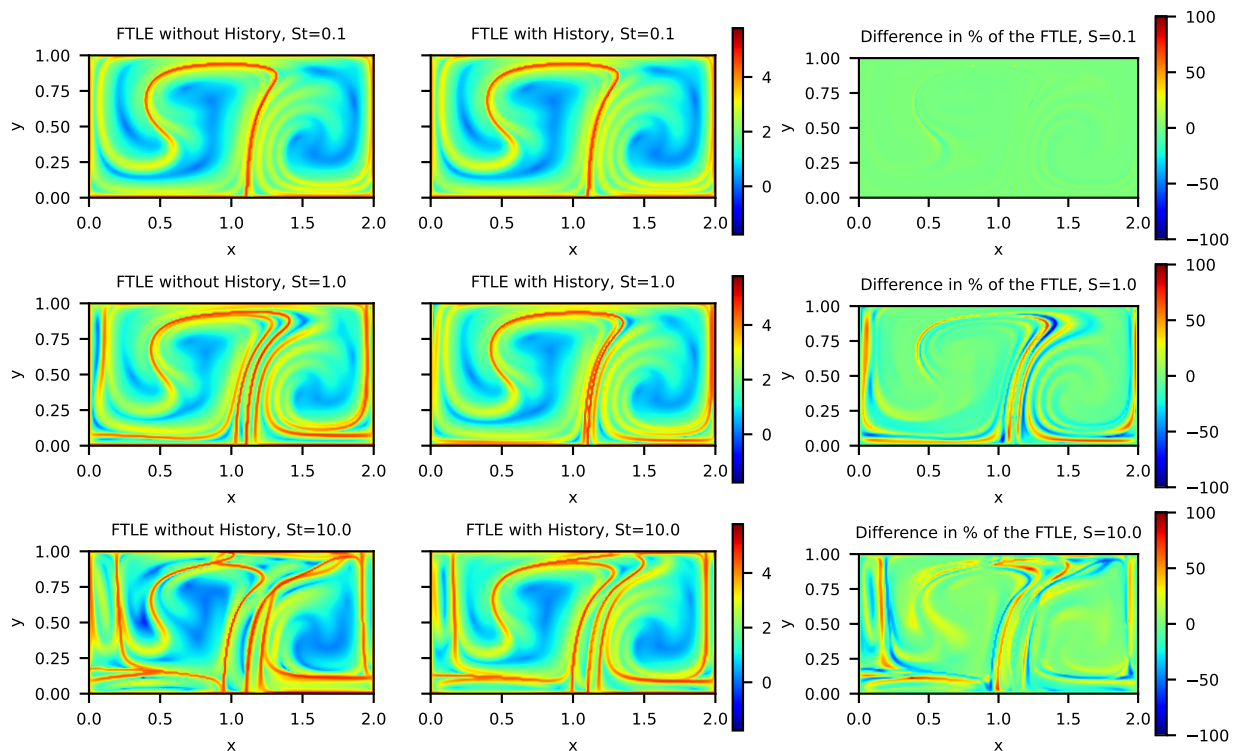


FIG. 7. FTLEs for heavy particles ($R = 11/9$) and three Stokes numbers, $S = 0.1$ (top), $S = 1$ (center), $S = 10$ (bottom), moving in the Double Gyre with periodic Boundary conditions. Left and center columns show the FTLEs computed with trajectories calculated without (left) and with (right) BHT. Right column shows the relative difference in the FTLE.

2. Bickley jet

Figures 8 and 9 shows the FTLE (left and center) and difference between FTLE with and without BHT (right) for the Bickley jet. Again, for both lighter- and heavier-than-fluid particles, the differences for $S = 0.1$ are mostly small, although a few localized regions emerge where shifts

in the position of divergence zones around the vortices lead to differences of over 50%.

This effect becomes more pronounced for $S = 1$ where the FTLE in the jet are now showing differences up to 100%. For lighter-than-fluid particles, knot-like objects structures emerge in regions of high curvature within the jet for the case $S = 1$ without BHT. While this looks like a numerical artifact on first sight, it can be well explained by the fact that particles initialized in the jet may leave it due to the inertial effects and may enter the neighborhood of one of surrounding vortices. This is also visible in the corresponding final particle positions: compare the central panels in Figure 4. Note that the high-FTLE structures for $S = 1$ computed without BHT are similar those computed for the higher Stokes number $S = 10$ with BHT.

Again, for $S = 10$, the differences increase and ignoring the BHT leads to a strong overestimation of FTLE of up to 100% in some parts. Even with BHT we now see the emergence of knot-like structures in the jet that were already observed for $S = 1$ without BHT.

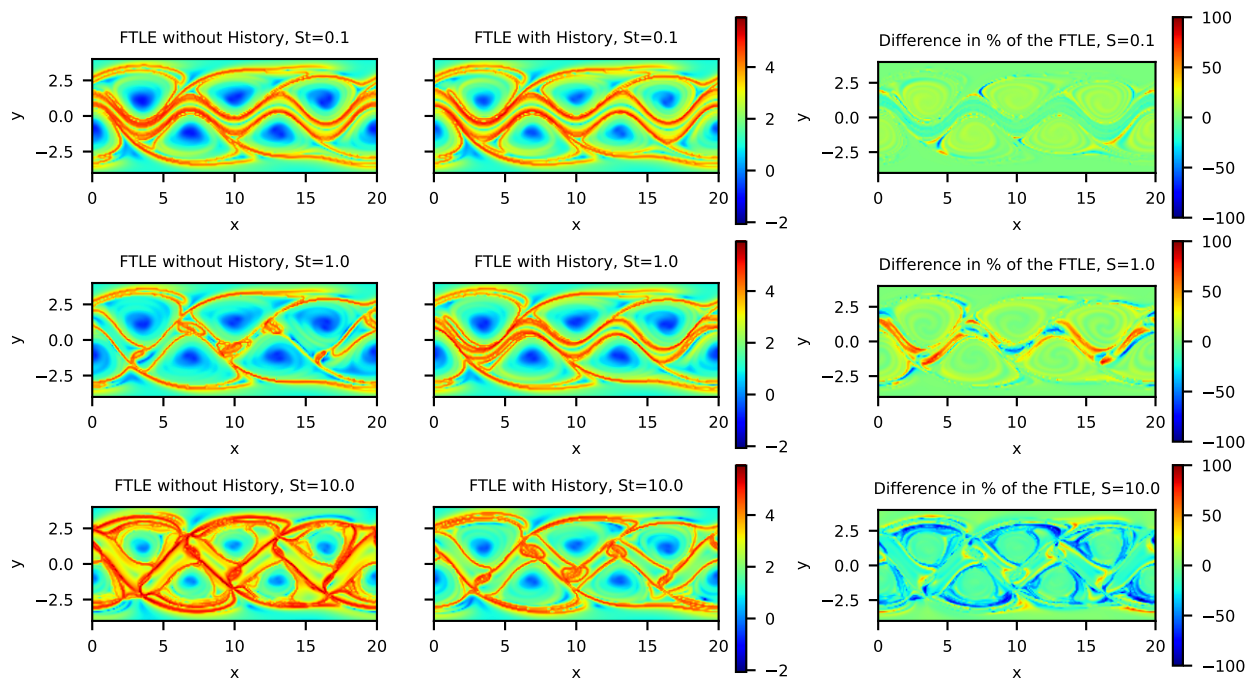


FIG. 8. FTLEs for light particles ($R = 7/9$) and three Stokes numbers, $S = 0.1$ (top), $S = 1$ (center), $S = 10$ (bottom), moving in the Bickley Jet. Left and center columns show the FTLEs computed with trajectories calculated without (left) and with (right) BHT. Right column shows the relative difference in the FTLE.

Relevance of the Basset history term for Lagrangian particle dynamics

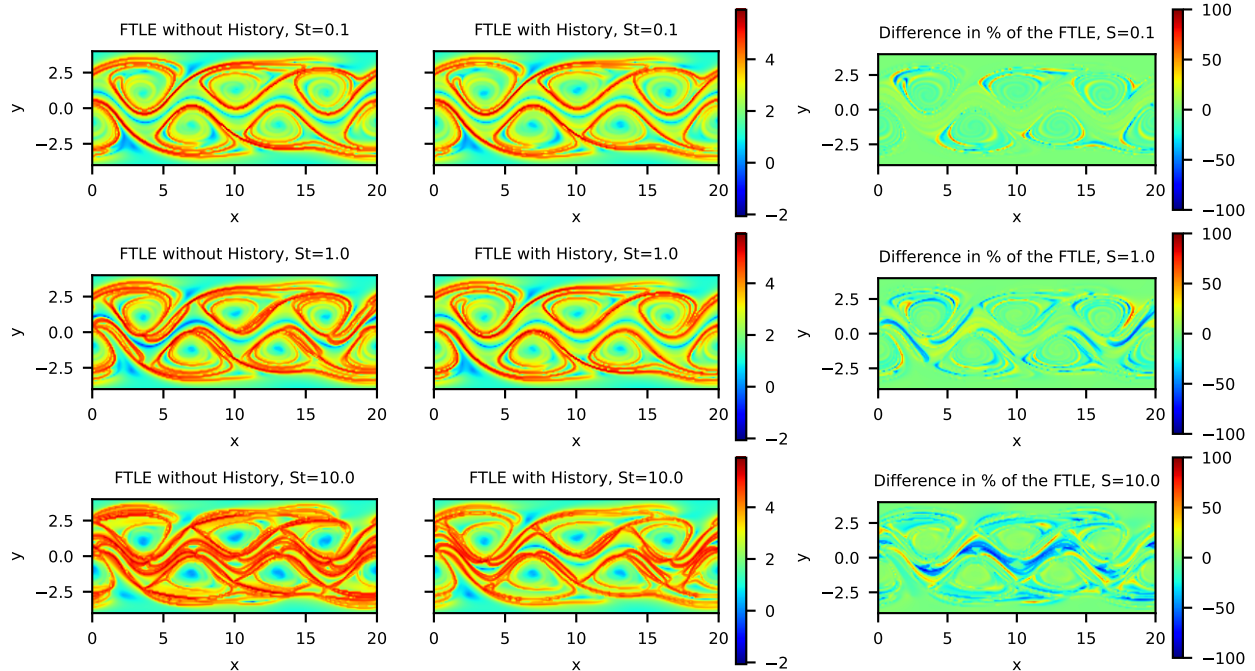


FIG. 9. FTLEs for heavy particles ($R = 11/9$) and three Stokes numbers, $S = 0.1$ (top), $S = 1$ (center), $S = 10$ (bottom), moving in the Bickley Jet. Left and center columns show the FTLEs computed with trajectories calculated without (left) and with (right) BHT. Right column shows the relative difference in the FTLE.

3. Faraday flow

Finally, figures 10 and 11 show the FTLE and differences between FTLE for the Faraday flow. For both $R = 7/9$ and $R = 11/9$ we see locally concentrated significant quantitative differences already for $S = 0.1$. The effect is more pronounced for the heavier-than-fluid particles where substantial regions with differences in the FTLE between 50 and 100% arise. Table I substantiates this observations, showing that, even on average, final particle positions are very different with and without BHT.

For $S = 1$ and both lighter and heavier particles, there are much larger zones with high, positive FTLEs without BHT than with. The effect is even stronger for $S = 10$ where throughout most of the domain the FTLE without BHT are larger than +5 whereas with BHT significant areas with smaller FTLE of around 2 – 3 remain. In both cases, the FTLE are overestimated by up to 100% when ignoring the BHT. This suggests that ignoring the BHT may lead to unrealistically effective mixing in simulations, because particles trajectories diverge too rapidly.

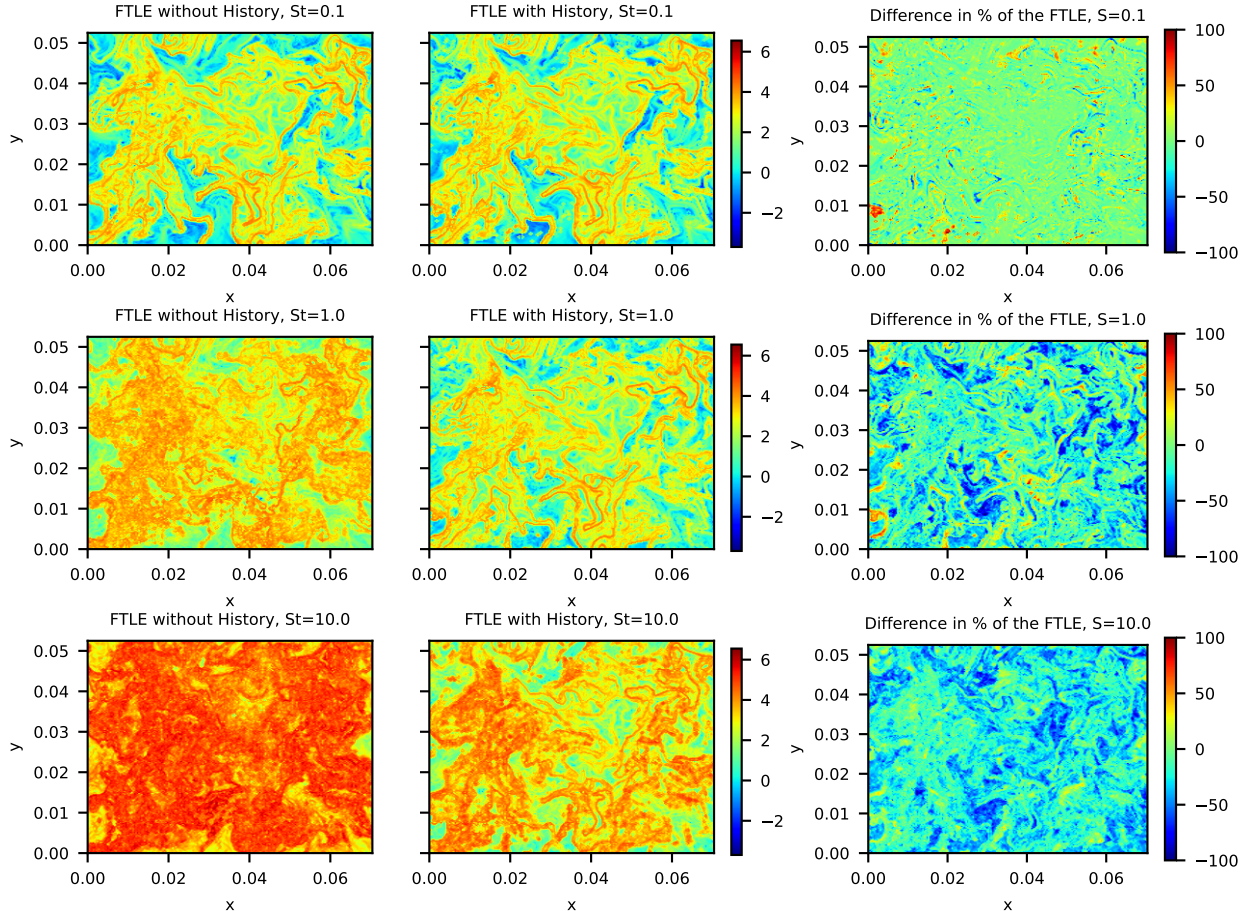


FIG. 10. FTLEs for light particles ($R = 7/9$) and three Stokes numbers, $S = 0.1$ (top), $S = 1$ (center), $S = 10$ (bottom), moving in the Faraday flow. Left and center columns show the FTLEs computed with trajectories calculated without (left) and with (right) BHT. Right column shows the relative difference in the FTLE.

V. CONCLUSIONS

We investigate how the Basset history term (BHT) in the Maxey-Riley equation changes the Lagrangian dynamics of simulated inertial particles. To this end, we solve the nondimensional Maxey-Riley equation with and without BHT for thousands of particles in three flow fields, a double gyre, the Bickley jet and an experimentally measured Faraday flow. We compare the clustering of the particles and finite-time Lyapunov exponents for trajectories computed with and without BHT.

For the double gyre and Bickley jet and a Stokes number of $S = 0.1$ we see little difference between the dynamics computed with and without BHT. Since the Faraday flow is more turbulent, even for $S = 0.1$ ignoring the BHT already has a visible impact on the FTLE field. For $S = 1$

Relevance of the Basset history term for Lagrangian particle dynamics

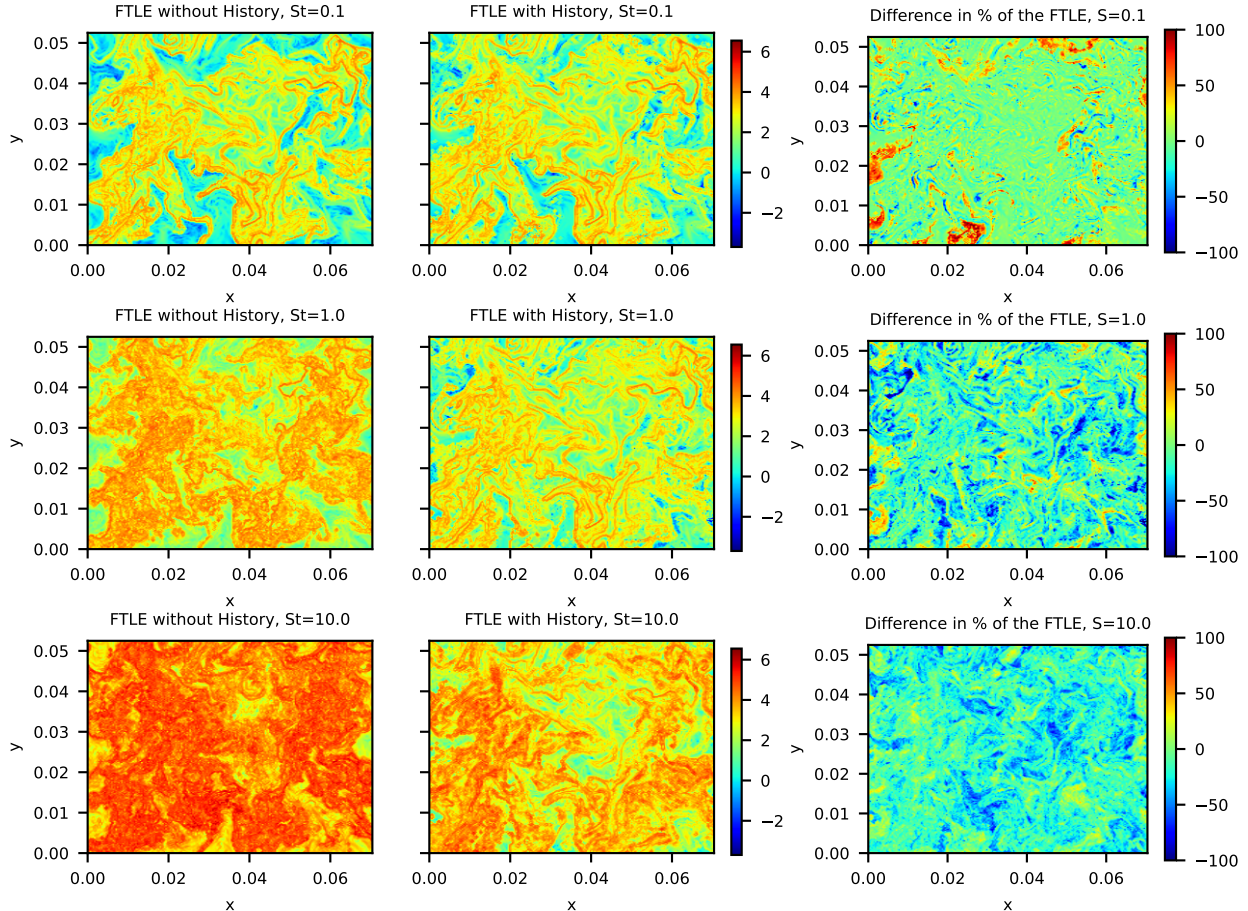


FIG. 11. FTLEs for heavy particles ($R = 11/9$) and three Stokes numbers, $S = 0.1$ (top), $S = 1$ (center), $S = 10$ (bottom), moving in the Faraday Flow. Left and center columns show the FTLEs computed with trajectories calculated without (left) and with (right) BHT. Right column shows the relative difference in the FTLE.

and even more so for $S = 10$, these significant difference also emerge for the double gyre and the Bickley jet. In line with previous findings, ignoring the BHT leads to an overestimation of ejection of particles from vortices in the flow. It also shifts the positions of areas of strong divergence, even when the overall patterns still look similar.

Generally, ignoring the BHT overestimates FTLE and leads to Lagrangian dynamics that would only be seen for a larger Stokes number if the BHT was considered. This also makes sense mathematically: with the BHT, the full history of the particle influences the forces acting on a particle at some given time. Without BHT, only the instantaneous forces due to the material derivative of the flow field and Stokes drag act on the particle. Therefore, without BHT, the forces from one time step to the next will change more drastically whereas the BHT adds a form of “mathematical

inertia” since the integral over the particle’s past trajectory changes more slowly and the acting forces and thus the particle’s speed and direction will change less rapidly.

In conclusion, our analysis backs up previous studies^{6,9,10} that demonstrate that the Basset history term cannot safely be ignored even when simulating comparatively small particles. It confirms that the differences matter not only at the level of individual particle trajectories but that also the larger scale Lagrangian dynamics change potentially significantly if the BHT is neglected. In particular, the overestimation of FTLE could lead to unrealistically efficient mixing in simulations when the BHT is ignored. Given that recent advances in numerical mathematics now allow for the efficient solution of the full MRE^{6,19,42}, we argue that simulations of inertial particles should routinely include the history term.

ACKNOWLEDGMENTS

This project is funded by the Deutsche Forschungsgemeinschaft (DFG, German Research Foundation) – SFB 1615 – 503850735.

DATA AVAILABILITY STATEMENT

AVAILABILITY OF DATA	STATEMENT OF DATA AVAILABILITY
Data openly available in a public repository that issues datasets with DOIs	The data that support the findings of this study are openly available at https://doi.org/10.5281/zenodo.12557890 .

REFERENCES

- ¹M. R. Maxey and G. L. Dent, in *Collective Dynamics of Particles*, Vol. 576, edited by C. Marchioli (Springer International Publishing, Cham, 2017) pp. 1–38, series Title: CISM International Centre for Mechanical Sciences.
- ²M. R. Maxey and J. J. Riley, *The Physics of Fluids* **26**, 883 (1983).
- ³P. Costa, L. Brandt, and F. Picano, *Journal of Fluid Mechanics* **891**, E2 (2020).
- ⁴E. E. Michaelides, *Physics of Fluids A: Fluid Dynamics* **4**, 1579 (1992).
- ⁵M. Farazmand and G. Haller, *Nonlinear Analysis: Real World Applications* **22**, 98 (2015).
- ⁶S. G. Prasath, V. Vasan, and R. Govindarajan, *Journal of Fluid Mechanics* **868**, 428 (2019).

- ⁷S. Olivieri, F. Picano, G. Sardina, D. Iudicone, and L. Brandt, *Physics of Fluids* **26**, 041704 (2014).
- ⁸A. Daitche and T. Tél, *New Journal of Physics* **16**, 073008 (2014).
- ⁹F. Candelier, J. R. Angilella, and M. Souhar, *Physics of Fluids* **16**, 1765 (2004).
- ¹⁰K. Guseva, U. Feudel, and T. Tél, *Phys. Rev. E* **88**, 042909 (2013).
- ¹¹G. Haller, *Annual Review of Fluid Mechanics* **47**, 137 (2015).
- ¹²M. R. Allshouse and T. Peacock, *Chaos* **25**, 097617 (2015).
- ¹³A. Hadjighasem, M. Farazmand, D. Blazeovski, G. Froyland, and G. Haller, *Chaos* **27**, 053104 (2017).
- ¹⁴A. Badza, T. W. Mattner, and S. Balasuriya, *Physica D: Nonlinear Phenomena* **444**, 133580 (2023).
- ¹⁵T. Sapsis and G. Haller, *Chaos: An Interdisciplinary Journal of Nonlinear Science* **20**, 017515 (2010).
- ¹⁶M. Sudharsan, S. L. Brunton, and J. J. Riley, *Phys. Rev. E* **93**, 033108 (2016).
- ¹⁷D. Garaboa-Paz and V. Pérez-Muñuzuri, *Nonlinear Processes in Geophysics* **22**, 571 (2015).
- ¹⁸T. Günther and H. Theisel, *IEEE Transactions on Visualization and Computer Graphics* **23**, 970 (2017).
- ¹⁹J. Urizarna-Carasa, L. Schlegel, and D. Ruprecht, arXiv preprint arXiv:2403.13515 (2024).
- ²⁰G. Haller, *Journal of Fluid Mechanics* **874**, 1–4 (2019).
- ²¹S. C. Shadden, F. Lekien, and J. E. Marsden, *Physica D: Nonlinear Phenomena* **212**, 271 (2005).
- ²²I. Rypina, M. G. Brown, F. J. Beron-Vera, H. Koçak, M. J. Olascoaga, and I. Udovydchenkov, *Journal of the Atmospheric Sciences* **64**, 3595 (2007).
- ²³R. Colombi, M. Schlüter, and A. v. Kameke, *Experiments in fluids* **62**, 1 (2021).
- ²⁴R. Colombi, N. Rohde, M. Schlüter, and A. von Kameke, *Fluids* **7**, 148 (2022).
- ²⁵F. J. Beron-Vera, M. J. Olascoaga, and P. Miron, *Physics of Fluids* **31**, 096602 (2019).
- ²⁶D. G. F. Huilier, *Fluids* **6**, 10.3390/fluids6040145 (2021).
- ²⁷A. Daitche, *Journal of Fluid Mechanics* **782**, 567–593 (2015).
- ²⁸M. Bourgoin, Some aspects of the collective dynamics of particles in turbulent flows, in *Collective Dynamics of Particles: From Viscous to Turbulent Flows*, edited by C. Marchioli (Springer International Publishing, Cham, 2017) p. 67–97.
- ²⁹N. T. Ouellette, P. J. J. O’Malley, and J. P. Gollub, *Phys. Rev. Lett.* **101**, 174504 (2008).
- ³⁰S. Hofmann, C. Weiland, J. Fitschen, A. von Kameke, M. Hoffmann, and M. Schlüter, *Chemical*

- Engineering Journal **449**, 137549 (2022).
- ³¹G. P. Langlois, M. Farazmand, and G. Haller, *Journal of nonlinear science* **25**, 1225 (2015).
- ³²K. Chong, S. D. Kelly, S. Smith, and J. D. Eldredge, *Physics of Fluids* **25**, 033602 (2013).
- ³³C. P. Cummins, O. J. Ajayi, F. V. Mehendale, R. Gabl, and I. M. Viola, *Physics of Fluids* **32**, 083302 (2020).
- ³⁴P. M. Lovalenti and J. F. Brady, *Journal of Fluid Mechanics* **256**, 561 (1993).
- ³⁵R. Mei, *Journal of Fluid Mechanics* **270**, 133 (1994).
- ³⁶A. Dorgan and E. Loth, *International journal of multiphase flow* **33**, 833 (2007).
- ³⁷P. A. Moreno-Casas and F. A. Bombardelli, *Environmental Fluid Mechanics* **16**, 193 (2016).
- ³⁸J. Klinkenberg, H. De Lange, and L. Brandt, *Meccanica* **49**, 811 (2014).
- ³⁹H. A. Elghannay and D. K. Tafti, *International Journal of Multiphase Flow* **85**, 284 (2016).
- ⁴⁰M. Parmar, S. Annamalai, S. Balachandar, and A. Prosperetti, *Journal of fluid mechanics* **844**, 970 (2018).
- ⁴¹M. Van Hinsberg, J. ten Thije Boonkkamp, and H. J. Clercx, *Journal of Computational Physics* **230**, 1465 (2011).
- ⁴²A. Daitche, *Journal of Computational Physics* **254**, 93 (2013).
- ⁴³M. N. Koleva, in *International Conference on Large-Scale Scientific Computing* (Springer, 2005) pp. 509–517.
- ⁴⁴U. M. Ascher, S. J. Ruuth, and R. J. Spiteri, *Applied Numerical Mathematics* **25**, 151 (1997).
- ⁴⁵P. Virtanen, R. Gommers, T. E. Oliphant, M. Haberland, T. Reddy, D. Cournapeau, E. Burovski, P. Peterson, W. Weckesser, J. Bright, S. J. van der Walt, M. Brett, J. Wilson, K. J. Millman, N. Mayorov, A. R. J. Nelson, E. Jones, R. Kern, E. Larson, C. J. Carey, Í. Polat, Y. Feng, E. W. Moore, J. VanderPlas, D. Laxalde, J. Perktold, R. Cimrman, I. Henriksen, E. A. Quintero, C. R. Harris, A. M. Archibald, A. H. Ribeiro, F. Pedregosa, P. van Mulbregt, and SciPy 1.0 Contributors, *Nature Methods* **17**, 261 (2020).
- ⁴⁶J. Urizarna-Carasa, *JulioUri/Basset-History-Term-Influence: Repo ready for submission* (2024), <https://doi.org/10.5281/zenodo.12557890>.
- ⁴⁷A. Hadjighasem, D. Karrasch, H. Teramoto, and G. Haller, *Physical Review E* **93**, 063107 (2016).
- ⁴⁸K. Padberg-Gehle and C. Schneide, *Nonlinear Processes in Geophysics* **24**, 661 (2017).
- ⁴⁹A. von Kameke, F. Huhn, G. Fernández-García, A. P. Muñozuri, and V. Pérez-Muñozuri, *Phys. Rev. Lett.* **107**, 074502 (2011).

Relevance of the Basset history term for Lagrangian particle dynamics

⁵⁰A. von Kameke, F. Huhn, A. P. Muñuzuri, and V. Pérez-Muñuzuri, *Phys. Rev. Lett.* **110**, 088302 (2013).

⁵¹P. Tallapragada and S. D. Ross, *Phys. Rev. E* **78**, 036308 (2008).